A SYSTEMATIC STUDY OF LASER ABLATION FOR SPACE DEBRIS MITIGATION

W.J. Burger[*1], **A. Cafagna**[2], **and C. Manea**[3]

[1]*FBK, Via Sommarive 18, and TIFPA, via Sommarive 14, 38123 Trento, Italy*
[2]*University of Trento and TIFPA, via Sommarive 14, 38123 Trento Italy*
[3]*TIFPA, via Sommarive 14, 38123 Trento, Italy*

ABSTRACT

The increase in the number of artificial objects in orbit around the Earth represents a serious threat to the future utilization of space. The scope and nature of the problem require an international effort. The Trento Institute of Fundamental Physics and Applications (TIFPA) participates in the study of laser ablation for space applications, propulsion and space debris mitigation, in the New Reflections program of the Italian *Instito di Fisica Nucleare* (INFN). An evaluation of the performance of laser ablation for debris removal in Low Earth Orbit (LEO), for different scenarios of ground-based and orbiting system configurations is presented. The results are obtained from a simulation developed in the Matlab© environment, which includes the relevant gravitational (Earth zonal model, solar and lunar gravity) and atmospheric models.

Key words: laser ablation, space debris mitigation, simulation analysis.

INTRODUCTION

The likelihood that the increase of the number of objects launched in space results in an artificial debris belt around the Earth was pointed out by D.J. Kessler and B.G. Cour-Palais in 1978 [1]. The authors developed a model to predict the evolution of the debris population created by satellite collisions based on the available inventory of artificial objects in orbit around the earth (size, speed, orbit). The process of mutual collisions is similar to the mechanism responsible for the creation of asteroids from larger planet-like bodies. While the time scale of the latter is of the order of billions of years, the much smaller volume occupied by the earth-orbiting satellites results in a significantly shorter time scale.

The authors indicate the inherent risk

Collisional breakup of satellites will become a new source for additional satellite debris in the near future, possibly well before the year 2000. Once collisional breakup begins, the debris flux in certain regions near earth may quickly exceed the natural meteoroid flux. Over a longer period the debris flux will increase exponentially with time, even though a zero net input rate may be maintained.

The *Kessler Syndrome*, the cascade in the number of collisions rendering the exploitation of space unfeasible for future generations, has led to a large consensus among national space agencies on the importance of the problem [2].

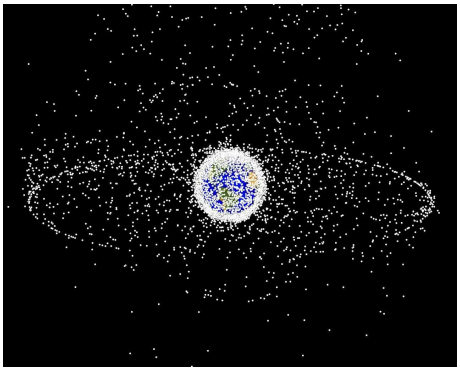

Figure 1. The principal space debris populations include a ring of objects in GEO and a cloud of objects in LEO [3].

The number of tracked objects, which exceeds 19,000. form two distinct populations: a ring in geostationary orbit (GEO) and a cloud in LEO (Fig.1). The information is used by NASA to defined collision avoidance processes for all human space flight missions and for maneuverable robotic satellites in LEO, and within 200 km of GEO [4].

The satellites and debris in orbit around the earth are subject to the frictional force of the atmosphere and the pressure due to solar activity. *A priori* the objects in LEO will eventually deorbit due to these natural effects. One of approaches in active debris removal is to search for technological solutions which would shorten significantly the orbital lifetime of the debris.

[*]corresponding author

REQUIRED PERFORMANCE

The impulse, applied in the direction opposite (parallel) to the orbital velocity, required to lower (raise) a object in a circular orbit is given by the Hohmann transfer. The momentum change is defined by the difference between the original orbital velocity, and the velocity at the perigee (apogee) of the elliptical transfer orbit tangent to the circle of the lower (higher) altitude orbit. The expression for the momentum change required to displace a mass m in an circular orbit of radius R_1 to an orbit radius $R_2 < R_1$ is

$$m\Delta v = MG \cdot \left(\sqrt{\frac{1}{R_1}} - \sqrt{2\frac{R_2/R_1}{R_1 + R_2}} \right) \qquad (1)$$

where M is the mass of the Earth and G is the gravitational constant.

The impulse required to lower the altitude of the satellite R_1 to R_2 equal to the Earth's radius[1] R_E, and $R_E + 150\,\mathrm{km}$ are shown in Fig. 12. The latter represents an altitude where the effect of atmospheric drag will deorbit the mass. The ratio of the impulse with and without atmospheric drag, i.e. the ratio of the impulses required to lower the mass to an altitude of 150 km and to the Earth's surface, are shown in Fig3.

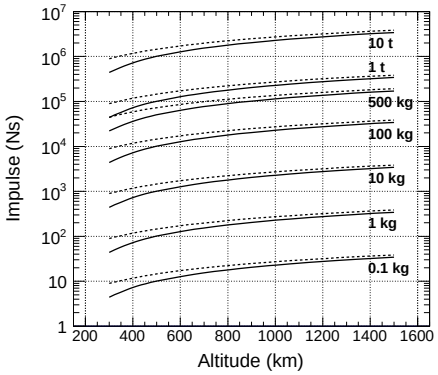

Figure 2. The impulse required to lower a given mass to a final orbital altitude of $150\,km$ (solid lines) and to the Earth's surface (dashed lines).

Effect of the Impulse Direction

The Geant4 application PLANETOCOSMICS was used to quantify the effect of the direction of the applied impulse. PLANETOCOSMICS performs a detailed simulation of the propagation and interaction of elementary particles in the Earth's magnetic field and atmosphere. The Earth's gravitational field was added to the program.

[1]Mean equatorial radius 6378 km

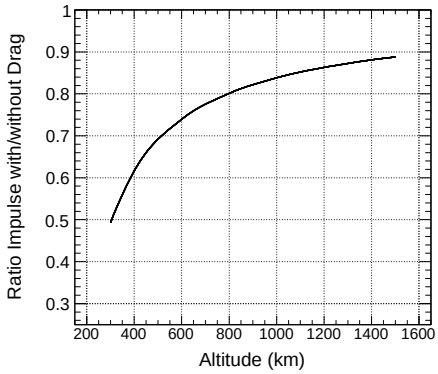

Figure 3. The ratio of the impulse required to deorbit the debris mass with and without the presence of the atmosphere.

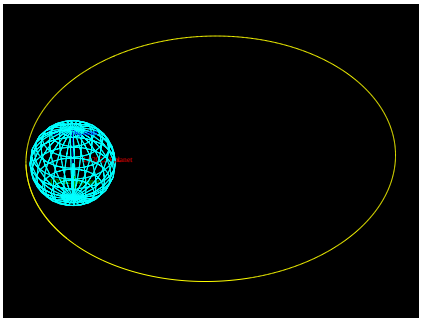

Figure 4. The elliptical orbit in the Geant4 simulation of the 500 kg mass with a velocity of 10.0 km/s. The trajectory correspond to 13 h, the period of an elliptical orbit with a semi-major axis equal to ~ 4 Earth radii.

Figures 4 and 5 show the orbits of a 500 kg mass which is placed at an altitude of 600 km with the velocities of 10.0 and 7.6 km/s. The corresponding escape velocity at this altitude is 11.2 km/s (Fig. 6).

The change of the perigee altitude produced by an impulse applied in the direction opposite to the orbital velocity (Hohmann), and in the directions along and opposite to the vector drawn from the Earth's center to the debris position at the 600 km altitude, are shown in Fig. 7.

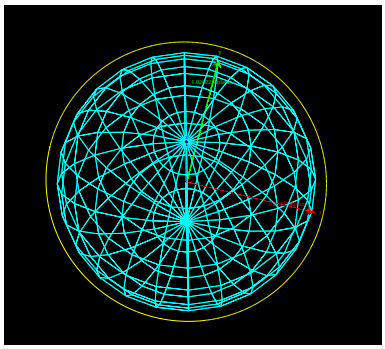

Figure 5. The circular orbit at altitude of 600 km of a 500 kg mass with a velocity of 7.6 km/s. The trajectory corresponds 97 min, the period of the circular orbit.

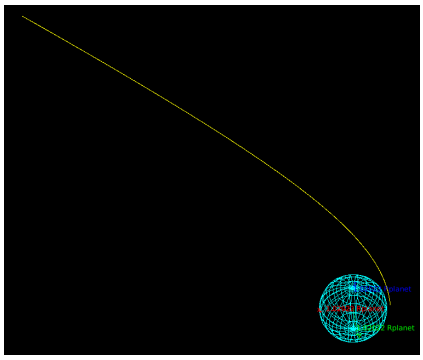

Figure 6. The trajectory of a 500 kg mass with a velocity of 11.2 km/s at an altitude of 600 km. The mass leaves the simulation volume at distance of 12 Earth radii with a velocity of 4.5 km/s in 4.2 h.

The simulation time is 97 min, corresponding to the period of the circular orbit of the 500 kg mass at an altitude of 600 km (Fig. 5). The impulse is applied 16.7 min after the start of the simulation. The effect of atmospheric drag is absent.

A factor ~ 4 larger radial impulse is required to produce a reduction in the perigee altitude comparable to the Hohmann transfer. The two radial impulses result in an elliptical orbit with a perigee altitude lower than the initial 600 km altitude of the initial circular orbit. The altitude reduction produced by the negative radial impulse is 5-10% larger.

The perigee time reported in Fig. 7 reflect the relative positions of the perigee and apogee of the elliptical orbits produced by the different impulse directions, illustrated in Figs. 8-10. The perigee altitude is attained $\sim 25\,\mathrm{min}$ after the negative radial impulse is applied; the perigee is displaced to the opposite side of the orbit with the positive radial impulse. The Hohmann transfer results in a perigee position lying between the two radially directed impulses.

The perigee altitude varies monotonically with the applied impulse below the value required to lower the 500 kg mass to the Earth's surface, $8.6 \cdot 10^4\,\mathrm{Ns}$ for the

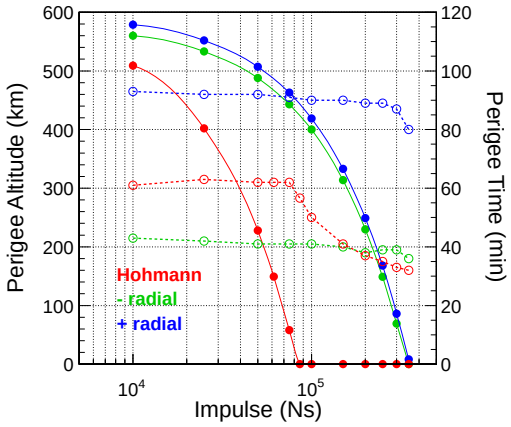

Figure 7. The change in the perigee altitude (●) for three different impulse directions: opposite to the orbital velocity of the 500 kg mass (Hohmann), towards the center of the Earth (negative radial) and the local zenith (positive radial) are indicated on the vertical axis on the left, the time required to attain the perigee (○) on the vertical axis on the right.

Hohmann transfer, and $3.5 \cdot 10^5\,\mathrm{Ns}$ for the two radial impulses. Above these values, the descent to the ground varies more rapidly with the impulse.

The simulation results in Fig. 7 are consistent with the impulse values of the Hohmann transfers (Eq. 1) of the 500 kg mass from 600 km to 150 km, $6.35 \cdot 10^4\,\mathrm{Ns}$, and to the Earth's surface, $8.6 \cdot 10^4\,\mathrm{Ns}$.

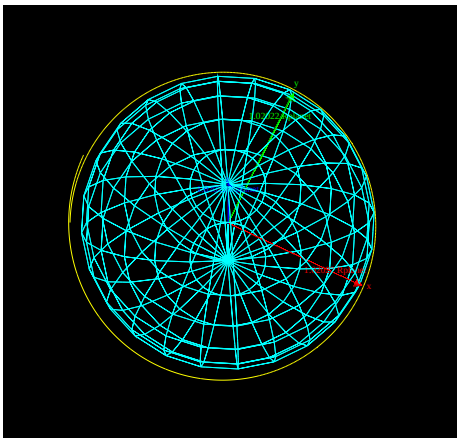

Figure 8. The modified trajectory of the 500 kg mass in a circular orbit at 600 km (Fig. 5) after the Hohmann transfer of $7.5 \cdot 10^4\,Ns$ in the direction opposite to its orbital velocity.

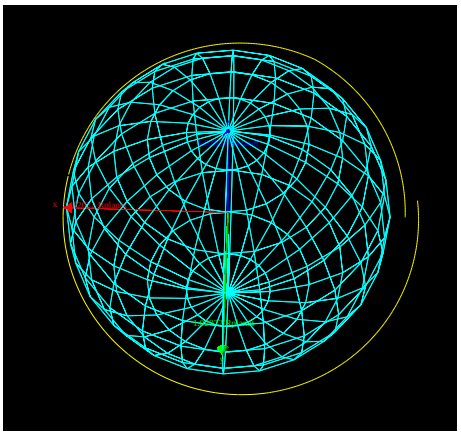

Figure 9. The modified trajectory of the 500 kg mass (Fig. 5) after the radial impulse of $3.0 \cdot 10^5\, Ns$ in the direction of the Earth's center.

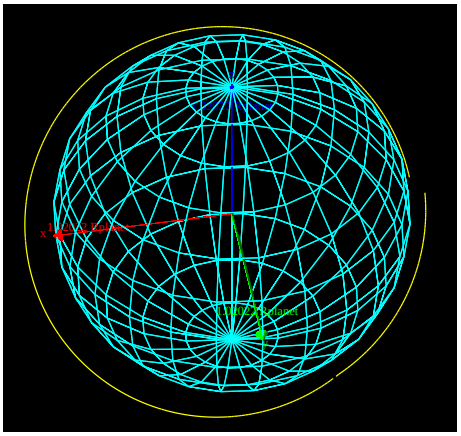

Figure 10. The modified trajectory of the 500 kg mass (Fig. 5) after the radial impulse of $3.0 \cdot 10^5\, Ns$ in the zenith direction.

Effect of Atmospheric Drag

The frictional force acting on a satellite due to the presence of the atmosphere is given by the expression,

$$\mathbf{F} = -\frac{1}{2}\rho C_D A v^2 \hat{\mathbf{v}} \qquad (2)$$

where ρ is the atmospheric density; C_D is the drag coefficient, which varies between 0 and 1; A and v are the satellite's cross-sectional area and velocity. The force acts in the direction opposite to satellite's orbital velocity.

The effect of the atmosphere on the orbit is introduced in the Geant4 simulation by adding the continuous energy loss process described by Eq. 2. The 500 kg debris mass is represented by a solid cube of aluminum with a surface area of $0.325\,\mathrm{m}^2$. The parameterizations for the troposphere, and the lower and upper stratospheres densities of Ref. [5] are used (Fig. 11).

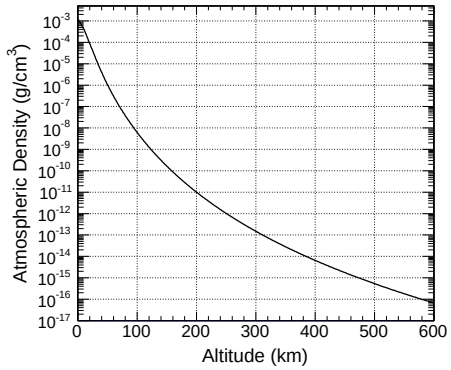

Figure 11. Atmospheric density from Ref. [5].

The effect of the atmospheric drag on the debris orbit for the three impulse directions is shown in Fig. 12. A Hofmann transfer of $4.0 \cdot 10^4\,\mathrm{Ns}$ results in a deorbit of the 500 kg mass in 5 y. The minimal values required to deorbit the mass are $1.75{\cdot}10^5$ and $2.0{\cdot}10^5\,\mathrm{Ns}$, respectively the negative and positive radial impulses; the corresponding deorbit times are 6.2 and 2.8 y.

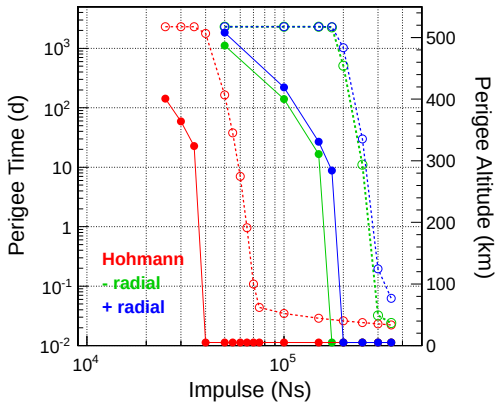

Figure 12. The perigee altitude (•) and time (○) for the three impulse directions with the presence of the atmosphere.

The perigee altitudes, 325-400 km for the Hohmann transfer and 285-508 km for the radial impulses, shown in Fig. 12 represent the altitudes attained after 6.34 y, the simulation time limit.

The Hohmann transfer applied to lower the perigee altitude is kinematically the optimal configuration. In practice, the impulse of a ground-based laser will always have a component directed away from the Earth. A space-based laser may engage debris targets at relatively lower and higher altitudes. The results for the radial direction transfers represent the performance lower limits.

The modified trajectory of the 500 kg mass after a

Hohmann transfer of $7.5 \cdot 10^4\ Ns$ in the direction opposite to its orbital velocity is shown in Fig. 13. The applied impulse results in a series of elliptical orbits with progressively lower perigee altitudes. When the altitude attains the height of the atmosphere each successive passage through the atmosphere produces a further reduction of the orbital velocity. The 500 kg mass falls to the Earth in 7 d after the initial Hohmann transfer.

The corresponding scenarios for negative and positive radial impulses of $2.5 \cdot 10^5$ Ns are illustrated in Figs. 14 and 15. The starting position of the debris mass is located in the equatorial plane at -600 km $\hat{\mathbf{x}}$.

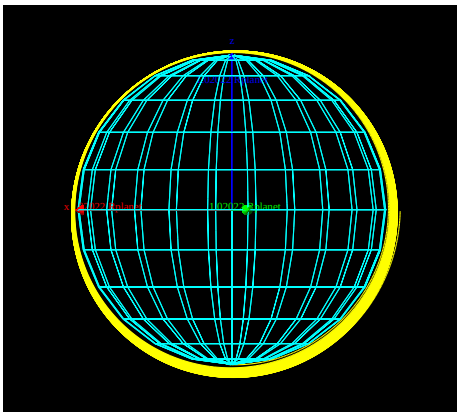

Figure 13. The 500 kg mass in a circular orbit at 600 km (Fig.5) returns to Earth 7 d after a Hohmann transfer of $6.0 \cdot 10^4$ Ns *and multiple passes in the atmosphere.*

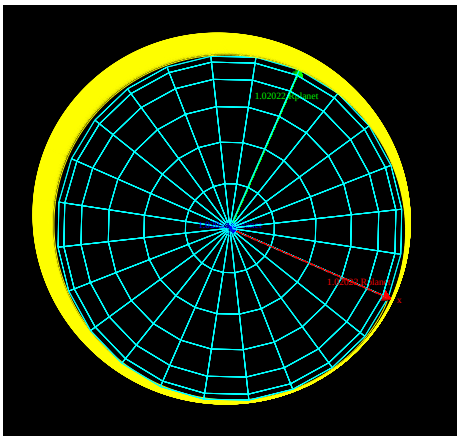

Figure 14. The 500 kg mass in a circular orbit at 600 km (Fig.5) returns to Earth 11 d after a negative radial impulse of $2.5 \cdot 10^5$ Ns *and multiple passes in the atmosphere.*

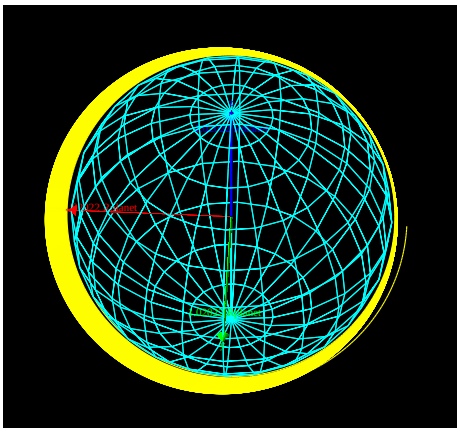

Figure 15. The 500 kg mass in a circular orbit at 600 km (Fig.5) returns to Earth 30 d after a positive radial impulse of $2.5 \cdot 10^5$ Ns *and multiple passes in the atmosphere.*

DEBRIS MITIGATION WITH LASER ABLATION

Ground-based System

A ground network of lasers for space debris removal is described in Ref. [6]. The quoted laser parameters are the energy per pulse $E_o > 10\,\mathrm{kJ}$, a repetition rate larger than 10 Hz, a pulse length between 1 and 50 ns, and a beam quality M2 less than 2.5. The expected power intensity at the surface of the debris is $0.1 - 0.8\,\mathrm{GW/cm^2}$. The impulse is given by the expression,

$$m\Delta v = \left(\frac{E_o T_{tel} T_{atm}}{\pi \phi^2(R)}\right) SC_m \tag{3}$$

where $\phi^2(R)$ is the size of the beam at the range R of the target debris. S and m are the surface area and mass of the target. T_{tel} and T_{atm} are the transmission efficiency of the laser emitting telescope and the atmosphere. C_m is the coupling coefficient (N/W) for the conversion of the incident laser pulse energy to kinetic energy.

The measured value of the coupling coefficient for aluminum is $\sim 2 \cdot 10^{-5}\,\mathrm{N/W}$ for the power density range between 0.5 and $0.8\,\mathrm{GW/cm^2}$, at $\lambda = 1.06\mu\mathrm{m}$. The vaporization threshold P_o for aluminum is $\sim 0.2\,\mathrm{GW/cm^2}$, below threshold $m\Delta v = 0$.

The atmospheric transmission is estimated using the Rozenberg model

$$T_m = (1 - A_{atm})^X \tag{4}$$

with

$$A_{atm} = 0.18 \text{ at } 1.06\,\mu\mathrm{m}$$

$$X = \frac{1}{cos\psi_Z + 0.025 \cdot e^{(-11 \cdot cos\psi_Z)}}$$

where ψ_Z is the elevation angle. Figure 16 shows the variation in the atmospheric transmission with the elevation angle for a $1.06\mu\mathrm{m}$ wavelength laser beam.

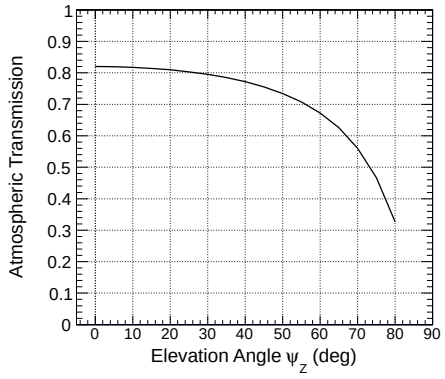

Figure 16. The variation of the transmission efficiency of the atmosphere for a $1.06\mu\mathrm{m}$ wavelength laser beam with the elevation angle, defined with respect to the zenith [6].

The performance has been evaluated for single and multiple pass modes. The results are sensitive to the parameters in Eq. 3, as well as to the tracking precision of the debris objects. The estimated deorbit times range from several hundreds of days to years. An object is considered deorbited once the perigee altitude reaches 150 km.

LASER DEPLOYMENT SCENARIOS

The Simulation

A simulation developed in Matlab© is used to study the relative performance of space and ground-based laser systems. Four laser deployment scenarios are evaluated: a dedicated satellite (SAT), a laser system installed on the International Space Station (ISS), and two ground-based systems located in the equatorial (GEQ) and polar (GPO) regions. The relative performance is evaluated for the same debris mass and orbit.

The debris is represented as a point mass M of 500 kg. Consequently, all forces act on the center-of-mass. The surface area A used for the computation of the frictional drag force is $5\,\mathrm{m}^2$, yielding a ballistic coefficient

$$\beta^* = C_D \cdot A/M = 0.1\,.$$

The laser beam delivers a 1 N thrust acting along the line-of-sight between the laser and debris positions. The beam is switched on and off in order to limit the time of operation to periods with advantageous orientations of the beam with respect to the debris velocity vector.

The laser is switched on when the debris approaches the ISS or satellite, and the line-of-sight between the space platform and debris is not obscured by the Earth, defined as a spherical volume with radius $R = R_E + 200\,\mathrm{km}$. For the ground-based systems, the laser is turned on when the object approaches the laser position, and the angle of elevation (Fig. 14) of the line-of-sight ψ_Z is greater than $65°$.

The Jacchia-Bowmann 2008 model [7] is used to calculate the air density at high altitudes. The model takes into account density fluctuations due to diurnal and seasonal thermal variations. The estimated accuracy of the computed densities is better than 4% based on comparisons with satellite accelerometer data. The epoch January 1, 2010, h.00:00:00.0 is chosen as the starting point in the simulation, in order to use known solar values for the calculation of the atmospheric density.

The debris orbital elements at epoch are listed in Table 1, which corresponds to an initial position at the apogee of the orbit (800 km). The chosen inclination and altitude is representative of the major part of the debris population in LEO.

Table 1. The orbital elements of the debris object at epoch: semi-major axis a, eccentricity e, inclination i, right ascension of the ascending node Ω, the argument of the perigee ω and the true anomaly θ.

a	e	i	Ω	ω	θ
7170 km	0.001	$100°$	$0°$	$180°$	$180°$

The orbital elements of the satellite and ISS at epoch are listed in Table 2. The starting point of the satellite is the perigee at an altitude of 500 km. The satellite altitude and inclination angle may be chosen to optimize the number of debris objects in its line-of-sight.

Table 2. The starting point orbit elements for the dedicated satellite and ISS scenarios.

	a	e	i	Ω	ω	θ
SAT	6885 km	0.001	$80°$	$180°$	$90°$	$0°$
ISS	6780 km	0.0016	$52°$	$128°$	$99°$	$313°$

The difference in altitude of the satellite and the debris object (Table 1) results in a relative rotation between their orbits due to the J_2 effect of the perturbed gravitational field. The rate of change in time (degree per mean solar day) of Ω, the Right Ascension of the Ascending Node (RAAN) is given by the expression [8]

$$\frac{d\Omega}{dt} = -\frac{9.9358}{(1-e^2)^2}\left(\frac{R_E}{R_E+\overline{h}}\right)^{3.5}\cos(i) \qquad (5)$$

where $\overline{h}$ is the mean distance from the Earth.

For the two circular orbits, with mean altitudes of 500 and 800 km, the difference in $\overline{h}$ results in an increase of $\Delta\Omega$ with time. The initially co-planar orbits will become again co-planar in ~ 980 days. All debris objects orbiting

at the same altitude, and similar, near polar inclinations, will be seen by the satellite in this time interval.

The time interval required to return to coplanarity for the higher altitude (1000-1500 km), near-polar orbit debris objects is shorter. Therefore, the dedicated satellite would be able to target a significant fraction of the near-polar orbit debris in less than 3 y. A laser system installed on the ISS will observe the near-polar orbit debris due to the lower inclination angle of the space station.

The position of the equatorial ground-based laser station at epoch is on the x-axis of the Earth Centered Inertial (ECI) reference system, which is drawn between Earth's center to the Sun, at a distance of 6378 km from the Earth's center. The polar region laser station is at a distance of 6357 km from the Earth's center, placed to have the debris ($i = 100°$) at its zenith at epoch. The orbital direction of the debris ($i > 90°$) is opposite to the rotation of the Earth, and to the orbital directions of the satellite and ISS (Table 2).

Results

The results for the four scenarios are presented in Table 3. The satellite (ISS) lasers provide the impulse required to lower the 500 kg mass at 800 kg, to the altitude of the atmosphere (200 km), in 3 weeks (3 months). The altitude decrease is significantly slower for the two ground-based lasers. At the end of the 2 month simulation time, the debris perigee altitude decreases by 20 and 75 km for the two ground-based lasers. The total impulse delivered by the polar site laser is a factor 5.5 higher.

Table 3. The total simulated time $\mathrm{t_{tot}}$*, total time laser on* $\mathrm{t_{laser}}$*, delivered impulse to debris and the final altitude at time* $\mathrm{t_{tot}}$*. The simulated time was limited to 60 d for the two ground-based laser scenarios.*

	$\mathrm{t_{tot}}$	$\mathrm{t_{laser}}$	Impulse	Alt. Final
	d	h	Ns	km
SAT	23.1	41.5	$1.5 \cdot 10^5$	200
ISS	92.9	66.0	$2.4 \cdot 10^5$	200
GEQ	60.0	2.3	$8.3 \cdot 10^3$	781
GPO	60.0	13.0	$4.7 \cdot 10^4$	723

The results in Table 3 may be compared to the impulse required by a Hohmann transfer to lower a 500 kg mass from 800 km to 200 km, $8.22 \cdot 10^4\,\mathrm{Ns}$. The impulses required for the space-based lasers to lower the 500 kg debris mass to the 200 km perigee altitude are factors 1.8 and 2.9 larger. The fractions of time on target, t_{laser}/t_{tot} in Table 3, are 0.074 (SAT) and 0.029 (ISS).

The orbital descent after 60 d obtained with the polar site, ground-based laser, 800 to 781 km, may be compared to the 165 d required to deorbit the 500 kg mass in a circular orbit at 600 km, after a Hohmann transfer of $5.0 \cdot 10^4\,\mathrm{Ns}$ (Fig. 12). The corresponding impulse applied in the positive radial direction in the Geant4 simulation lowers the perigee altitude from 600 to 505 km in 6.34 y.

Required Laser Performance

The impulses quoted in Table 3 represent the sum of the impulse steps delivered each second by the 1 N laser thrust. The corresponding required energy E_o can be estimated from Eq. 3 with $m\Delta v = 1\,Ns$. For the space-based lasers ($T_{atm} = 1$),

$$E_o = \left(\frac{1\,\mathrm{Ns}}{T_{tel} \cdot C_m}\right)\left(\frac{S}{\pi\phi^2(R)}\right). \qquad (6)$$

The second term in Eq. 6 is the ratio of areas of the debris surface and laser beam spot at the target. With the debris surface of $5\,\mathrm{m}^2$, a 1 m diameter circular beam spot and a telescope transmission efficiency of 80%, E_o is 400 kJ, the average power 400 kW.

Figure 17 shows the variation of the pulse energy and peak power with repetition rate of the 400 kW laser, for a 5 ns pulse width. The laser peak power is plotted against the peak power density at the target in Fig. 18. The variation of the same parameters with the pulse width of the 400 kW laser, for a 5 Hz repetition rate, is shown in Fig. 19.

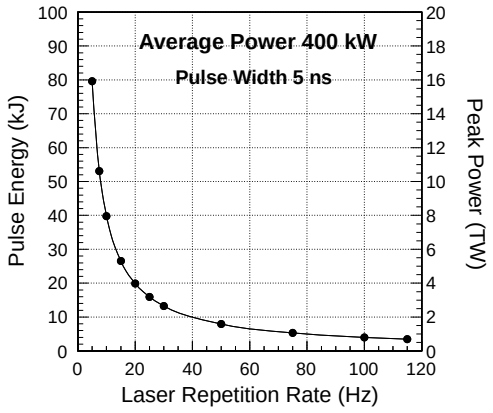

Figure 17. The variation with repetition rate of the pulse energy and peak power of the 400 kW space-based laser with a pulse width of 5 ns.

The minimum power density required to produce a momentum transfer by the vaporization of the material on the surface of the debris (Al) is $0.2\,\mathrm{GW/cm^2}$ Ref. [6]. The laser configurations with peak power densities lower than $1\,\mathrm{GW/cm^2}$ are indicated in red in Figs. 18 and 19.

A 400 kW, space-based laser would provide the time-integrated impulse compatible with the performance presented in Table 3. Two possible laser configurations, which provide the necessary power density at the target are a relatively low peak power, are listed in Table 4. Lower pulse energy E_o is obtained with a higher repetition rate and narrower pulse width.

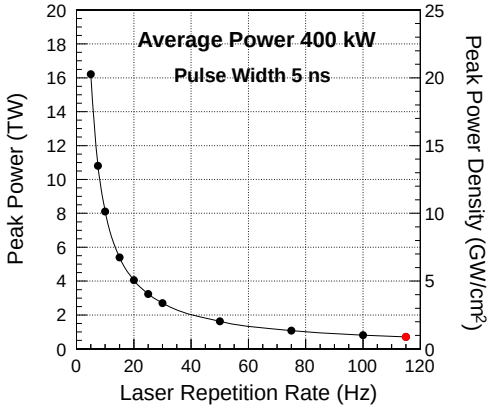

Figure 18. The variation of the peak power and the peak power density at the target with pulse width, for a 5 Hz repetition rate and an average power of 400 kW. Peak power densities below $1\,\mathrm{GW/cm^2}$ *are indicated in red.*

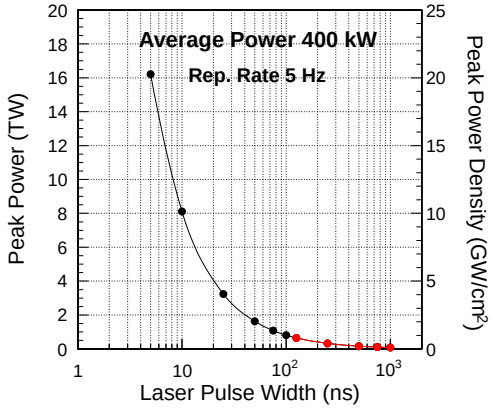

Figure 19. The variation of the peak power and the peak power density at the target with repetition rate, for a 5 ns pulse width and an average power of 400 kW. Peak power densities below $1\,\mathrm{GW/cm^2}$ *are indicated in red.*

Table 4. Laser configurations compatible with the performance of the space-based lasers in the Matlab© simulation (Table 3).

P_{avg}	E_{pulse}	P_{peak}	width	rate	$P_{density}$
kW	kJ	TW	ns	Hz	$\frac{GW}{cm^2}$
400	8.0	1.6	5	50	2.0
400	80	1.6	50	5	2.0

CONCLUSION

An estimate of the required performance for debris mitigation is obtained from the Hohmann transfer required to change the orbital altitude of a satellite. In contrast to a Hohmann transfer, the momentum transferred by a ground or space-based laser will not be concentrated in the direction opposite to the orbital velocity of the debris mass.

The Geant4 simulation was used to compare the perigee altitude of the Hohmann transfer with the altitude change produced by radial impulses directed along, and opposite to the vector drawn from the Earth's center to the debris position, the latter considered as limits for effective operation. A factor ~ 4 larger radial impulse is required to produce a comparable altitude change. Consequently, for a given intensity, the relative performance would be expected to vary from 1 to 0.25 depending on the relative positions of the laser and debris target.

A first estimate of the required laser characteristics is based on the results of the Matlab© simulation, which takes into account the oblateness of the Earth on the gravitational field, and the diurnal and seasonal thermal variations affecting the atmosphere density.

The 1 N thrust of the space-based lasers lower the perigee altitude of a 500 kg mass from 800 to 200 km, sufficient to produce a deorbit in the atmosphere, in a time varying between 3 weeks and 3 months depending on the laser orbit. The time-integrated impulse required is $1.5\text{-}2.4 \cdot 10^5\,\mathrm{Ns}$.

The corresponding laser energy $E_\circ$ is computed (Eq. 6) with the coupling coefficient and threshold peak power density of the $1.06\mu\mathrm{m}$ infrared laser reported in Ref. [6], and a 1 m diameter beam spot at the target. The average power required is 400 kW. Two pulsed laser configurations are listed in Table 4.

REFERENCES

[1] *Collision Frequency of Artificial Satellites: The Creation of a Debris Belt*, Journal of Geophysics Research, Vol 83, No. A6, 1979, 2637-2646.

[2] Inter-Agency Space Debris Coordination Committee: www.ladc-online.org

[3] NASA Orbital Debris Program Office: orbitaldebris.jsc.gov/index.html

[4] *The Threat of Orbital Debris and Protecting NASA Space Assets from Satellite Collisions* images.spaceref.com/news/2009/ODMediaBriefing28Apr09-1.pdf

[5] NASA Earth Atmosphere Model, http://www.grc.nasa.gov/WWW/k-12/airplane/atmos.html

[6] *Changes of Space Debris Orbits after LDR Operation* E. Wnuk, J. Golebiewska, C. Jacquelard, and H. Haag CLEANSPACE project of EC Seventh Framework Programme (FP7)

[7] *Jacchia-Lineberry Upper Atmosphere Density Model*, NASA Lyndon B. Johnson Space Center, 1982
A NEW Empirical Thermospheric Density Model JB2008 Using New Solar and Geomagnetic Indices, B. R. Bowman *et al.*, AIAA 2008

[8] *Orbital Mechanics*, V. A. Chobotov, AIAA 2002

[9] *Removing orbit debris with laser*, C. R. Phipps *et al.* Advances in Space Research 49, 2012

APPENDIX: ORBITAL ELEMENTS

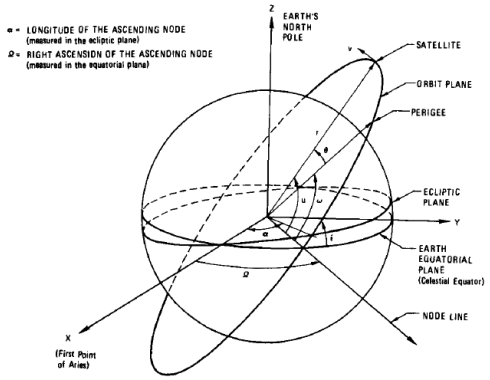

Fig. 3.5 Orientation of orbit in space (from Ref. 2).

Figure 20. The orbital elements inclination i, right ascension of ascending node Ω, the argument of the perigee ω and the true anomaly θ.